Earthquake Research Advances 6 (2026) 100397

Contents lists available at ScienceDirect

Earthquake Research Advances

journal homepage: www.keaipublishing.com/en/journals/earthquake-research-advances

Coulomb stress transfer from the 2025 M_W 7.7 Myanmar earthquake to active faults in southwestern Yunnan, China: Implications for seismic hazard

Yujiang Li*, Cheng Yang, Xingping Hu, Jie Yuan, Rui Yao, Hong Li

National Institute of Natural Hazards, Ministry of Emergency Management of China, Beijing, 100085, China

A B S T R A C T

On 28 March 2025, a strong M_W 7.7 earthquake struck the seismic gap in the central section of the Sagaing Fault in Myanmar, causing significant damages and casualties in Myanmar and neighboring countries. Major earthquakes like this are expected to transfer stresses to nearby active regions and change their seismic hazards in the near future. In this study, based on a stratified viscoelastic model and a coseismic slip model, we calculated the co- and post-seismic Coulomb stress change ($\triangle CFS$) imparted by the M_W 7.7 Myanmar earthquake to the main active faults in the adjacent southwestern Yunnan region in China. Our results show that five fault segments experience up to 3 kPa of coseismic stress increase, including the Longling-Lancang Fault, the Nantinghe Fault, the Menglian Fault, the Heihe Fault, and the Red River Fault, respectively. The pattern of postseismic $\triangle CFS$ is similar to that of coseismic $\triangle CFS$, suggesting that with the increasing elapsed time, the stress level continues to increase in these fault zones. The coseismic auxiliary stress fields show that the orientation of the principal tensile stress is predominantly NE-SW in the northern part of the southwestern Yunnan region, and shows clockwise rotation to NW-SE in the south. This stress regime controls the additional slip motion, consistent with that reflected by the coseismic shear stress change. Combined with other geophysical and geodetic data, we propose that more attention should be paid to the Longling-Lancang Fault, the Nantinghe Fault, the Menglian Fault, and the Heihe Fault, potential candidates for the next strong earthquakes in this region.

1. Introduction

On 28 March 2025, a M_W 7.7 earthquake struck the Sagaing Region of Myanmar, with an epicenter close to Mandalay, the country's second largest city. This strong event ruptured the seismic gap along the dextral Sagaing Fault (Hurukawa and Maung Maung, 2011; Tun and Watkinson, 2017), a plate boundary fault between the Burma and Sunda plates. Ground surface mapping and other geophysical and remote sensing analysis revealed that the unusual surface rupture distance produced by this supershear rupture extends ~500 km (Bradley and Hubbard, 2025; Inoue et al., 2025; Peng et al., 2025). The Sagaing Fault is entirely located in Myanmar, extending more than 1 200 km, and connects the Andaman spreading center to an oblique collision zone in the north (Curray, 2005; Wang et al., 2014). GPS observations indicate that strike-slip motion on the Sagaing fault varies between 18 mm/a and 49 mm/a (Le Dain et al., 1984; Lindsey et al., 2023; Maurin et al., 2010; Tin et al., 2022; Vigny et al., 2003), which accommodates more than half of the dextral motion between Sundaland and India within a diffuse plate boundary along the eastern margin of India (Panda et al., 2018; Socquet et al., 2006).

The Sagaing Fault has witnessed several strong historic earthquakes. Since 1906, more than ten $M \geq 6.7$ earthquakes have occurred on the Sagaing Fault (Kundu and Gahalaut, 2012), including the M_W 6.8 Thabeikky earthquake in 2012 and the recent M_W 7.7 Myanmar earthquake (Bradley and Hubbard, 2025; Peng et al., 2025). The occurrence of the M_W 7.7 Myanmar earthquake releases the highest accumulated stress and strain energy (Panda et al., 2018; x; Xiong et al., 2017), and meanwhile is expected to transfer stress to the adjacent southwestern Yunnan region with high-populated cities and a historical record of large earthquakes. More importantly, the seismic activity in the southwestern

* Corresponding author.
E-mail address: yujiangli@ninhm.ac.cn (Y. Li).

Peer review under the responsibility of Editorial Board of Earthquake Research Advances.

Production and Hosting by Elsevier on behalf of KeAi

https://doi.org/10.1016/j.eqrea.2025.100397
Received 8 April 2025; Received in revised form 3 June 2025; Accepted 3 June 2025

Yunnan region has been relatively quiet following the M 7.1 Menglian earthquake in 1995 (Li et al., 2020a), and thus the seismic hazards on the main active fault in this region are of great concern.

Coulomb stress change (ΔCFS) has been the primary physical principle used to explain the triggered earthquakes and is widely used in seismic hazard analysis (e.g., Hall, 2023; King et al., 1994; Li et al., 2023; Li et al., 2021; Li et al., 2020b; Nalbant et al., 2002; Parsons et al., 2008; Shan et al., 2013; Shao et al., 2016; Stein, 1999; Stein et al., 1997; Wan et al., 2000; Xiong et al., 2017). Based on the stress evolution along the North Anatolian fault zone, Stein et al. (1997) and Nalbant et al. (1998) identified regions that host large earthquakes along the northwestern segment of the fault. And the destructive 1999 Izmit M 7.4 earthquake indeed occurred in this segment (Hubert-Ferrari et al., 2000). Before the Myanmar earthquake, Xiong et al. (2017) calculated the stress evolution along the Sagaing Fault and identified the sections of the fault (seismic gaps) that most promoted failure earthquakes on the Sagaing Fault. As expected, the M_W 7.7 Myanmar earthquake on March 28 finally broke the central segment with the highest accumulated stress. x issued a one-month short-term earthquake forecast in western Myanmar based on the Coulomb stress changes ΔCFS from the M_W 7.7 mainshock. Peng et al. (2025) also examined how aftershocks and triggered seismicity near the Myanmar/Thailand borders were affected by both static and dynamic stress changes from the mainshock. Thus, in this study, we focused on the stress imparted by the M_W 7.7 Myanmar earthquake to the main active faults in the adjacent southwestern Yunnan region in China.

To address the aforementioned question, we collected the coseismic slip rupture model and calculated the co- and post-seismic ΔCFS imparted by the M_W 7.7 Myanmar earthquake on the adjacent major faults. Then, we analyzed seismic interaction and identified the fault segments that experienced high-stress change. Finally, we analyzed the coseismic auxiliary principal stress fields, which deepened our understanding of the mechanics that drive the fault stress change and fault slip motion.

2. Tectonic setting

Continental China and its adjacent region were divided into six first-order active tectonic blocks (Zhang et al., 2003), including the Yunnan-Myanmar block (Fig. 1). This block is situated along the southeastern margin of the Qinghai-Xizang Plateau, which is bounded by the large-offset dextral Sagaing Fault in Myanmar to the west and the large-scale dextral Red River Fault to the east (Shi et al., 2018; Taylor and Yin, 2009). Myanmar straddles the complex oblique plate boundary between the India Plate and Sundaland, the SE promontory of the Eurasia plate (Nielsen et al., 2004), and developed the dominantly dextral strike-slip Sagaing Fault (Rangin et al., 2013). Tectonic stress inversion shows that the stress regime around the epicenter of the Myanmar earthquake is strike-slip dominated (Hu et al., 2017), and the orientation of the maximum principal compressive stress is predominantly NE-SW, which controlled the dextral strike-slip of the Myanmar earthquake along the vertical Sagaing Fault.

As part of the Yunnan-Myanmar block, the southwestern Yunnan region dominated the lateral strike-slip motion, featuring a dominant series of the NE-trending arcuate sinistral strike-slip faults (Fu et al., 2011), and a subordinate set of NW-NWW trending dextral strike-slip faults (Shi et al., 2018). In particular, the predominant NE-trending sinistral faults included the Dayingjiang Fault, the Ruili-Longling

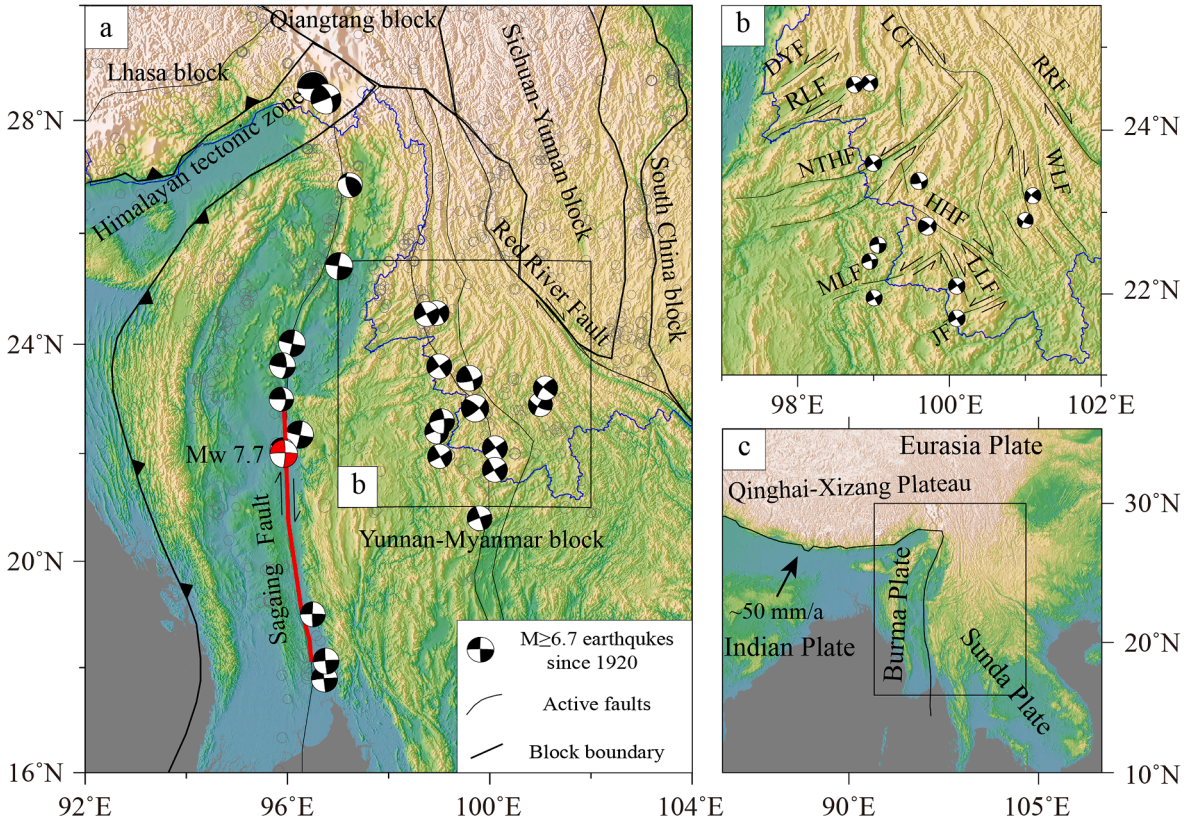

Fig. 1. (a) Tectonic setting and seismic activity within and around the Yunnan-Myanmar block. The black circles represent the historic $M \geq 5.0$ earthquakes since 1900 (Li et al., 2020a). The square marks the study region that is shown in (b). The red line denotes the coseismic rupture length of ~500 km of the M_W 7.7 Myanmar earthquake, according to the United States Geological Survey (USGS). (b) A zoom-in plot showing multiple faults and historical earthquakes near the Myanmar/China border. DYF, Dayingjiang Fault; HF, Heihe Fault; JF, Jinghong Fault; LCF, Lancang River Fault; LLF, Longling-Lancang Fault; MF, Menglian Fault; NF, Nantinghe Fault; RLF, Ruili-Longling Fault; RRF, Red River Fault; WF, Wuliangshan Fault. (c) A zoom-out plot showing the regional tectonic settings in East and Southeast Asia. The square marks the region plotted in (a).

Fault, the Nantinghe Fault, the Menglian Fault, and the Jinghong Fault; while the subordinate NW-NWW-trending dextral faults include the Longling-Lancang Fault, the Heihe Fault, and the Wuliangshan Fault (Fig. 1b). These conjugated fault systems jointly accommodated the relative motion and controlled the regional seismic activity in the southwestern Yunnan region.

In the past century, the southwestern Yunnan region experienced more than 10 $M \geq 6.7$ earthquakes following the M 6.9 Gengma earthquake in 1941. Seven of these events were of $M \geq 7.0$, including the two devastating Longling doublets in 1976 and the Lancang-Gengma doublets in 1988 (Wu et al., 2007). However, the seismic activity in this region has been relatively quiet following the M 7.1 Menglian earthquake in 1995, and no magnitude ≥ 7 earthquake has occurred since then (Li et al., 2020a).

3. Data and methods

3.1. Data and parameters

Shortly after the Myanmar earthquake, the USGS released multiple versions of the coseismic slip distribution, based on finite-fault inversions of the near-field strong motion recording, teleseismic waves, and geodetic observations. The latest version shows that the rupture plane includes 4 segments, with the total coseismic rupture length extended about 500 km, and the peak amplitude of the slip exceeds 4.0 m (https://earthquake.usgs.gov/earthquakes/eventpage/us7000pn9s/finite-fault). Additional studies based on back-projection of teleseismic waves and remote sensing revealed up to 480 m of co-seismic slip (Peng et al., 2025). Here, we use the openly available USGS finite-fault model to perform subsequent analysis.

We employed the PSGRN/PSCMP code (Wang et al., 2006), to calculate the co- and post-seismic $\triangle CFS$ imparted by the Myanmar earthquake to the adjacent receiving faults in the southwestern Yunnan region. The parameters used in the viscoelastic model (Fig. 2) and the parameters of the receiving fault geometry (Table S1) are consistent with Li et al. (2020a).

3.2. Method

The $\triangle CFS$ was calculated based on the Moho-Coulomb failure criteria (Harris, 1998; Stein, 1999),

$$\Delta CFS = \Delta\tau + \mu' \Delta\sigma_n \tag{1}$$

where $\Delta\tau$ is the shear stress change (positive in the fault slip direction), $\Delta\sigma_n$ is the normal stress change (positive for fault unclamping), and μ' is the apparent friction coefficient, which takes into account reductions in friction due to pore pressure changes.

To simulate transient elastic response, short exponential decaying time response, and long linearly increasing time response (Shao et al., 2016; Wang et al., 2012), we chose the Burgers model as the constitutive relation,

$$\sigma + \left(\frac{\eta_2}{k_1} + \frac{\eta_1}{k_1} + \frac{\eta_2}{k_2}\right)\dot{\sigma} + \frac{\eta_1\eta_2}{k_1k_2}\ddot{\sigma} = \eta_2\dot{\varepsilon} + \frac{\eta_1\eta_2}{k_1}\ddot{\varepsilon} \tag{2}$$

where σ and ε represent the stress and strain, k_1 and k_2 represent Young's modulus of the Kelvin model and Maxwell model, η_1 and η_2 are the transient and steady-state viscosity coefficients, respectively.

We calculated the co- and post-seismic $\triangle CFS$ imparted by this event at a depth of 10 km to the adjacent major faults in the southwestern Yunnan region, assuming the apparent friction coefficient $\mu' = 0.4$.

4. Results

4.1. Co- and post-seismic $\triangle CFS$ on main active faults in southwestern Yunnan region

Our preliminary results show that five fault segments experienced a significant coseismic stress increase (Fig. 3), corresponding to the Longling-Lancang Fault, the Nantinghe Fault, the Menglian Fault, the Heihe Fault, and the Red River Fault, respectively, in which the coseismic $\triangle CFS$ reaches 3 kPa, suggesting the increased seismic hazard on these fault segments. On the other hand, this event generated

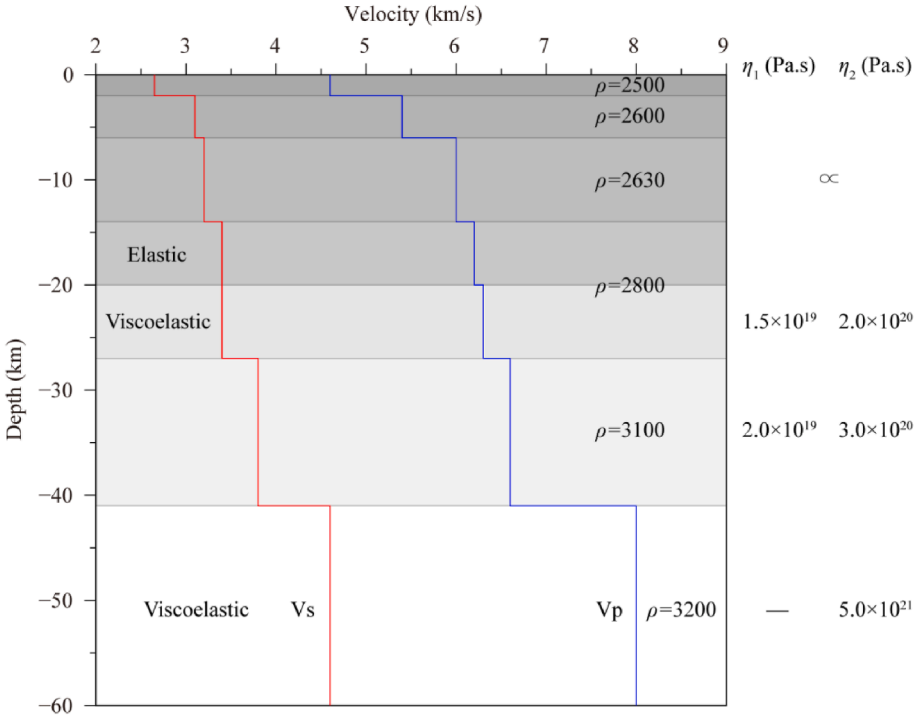

Fig. 2. Stratified parameters in the viscoelastic relaxation model.
V_p and V_s represent the P and S wave velocities, ρ is the lithospheric density, η_1 and η_2 are the transient and steady-state viscosities, respectively.

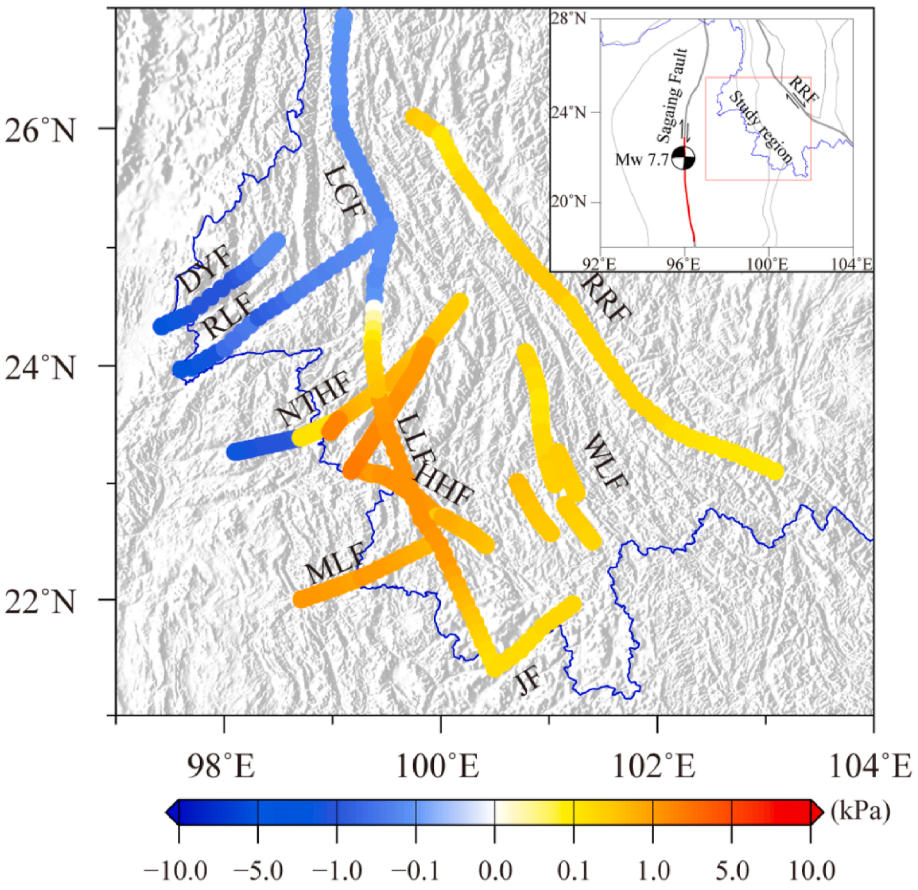

Fig. 3. Coseismic $\triangle CFS$ on main active faults in southwestern Yunnan region ($\mu' = 0.4$). The inset in the top right marks the study region with respect to the M_W 7.7 mainshock and the Sagaing fault. The red line denotes the coseismic rupture length of ~500 km of the M_W 7.7 Myanmar earthquake.

negative Coulomb stress changes on the Dayingjiang Fault, the Ruili-Longling Fault, and the Lancangjiang Fault.

To understand the contribution of the normal stress change and the shear stress change to $\triangle CFS$, we further analyze the stress components on the fault plane. We found that the main active faults in southwest Yunnan experienced a coseismic tensile normal stress change due to the Myanmar earthquake (Fig. 4). For the three faults with significant coseismic stress decrease (Fig. 3), the magnitude of the negative coseismic shear stress change is larger than the coseismic normal stress change, and thus the shear stress change is the main factor in the coseismic $\triangle CFS$. On the other fault planes, with the increase of the apparent friction coefficient μ', the contribution of the normal stress change to $\triangle CFS$ is increased.

With the postseismic viscoelastic relaxation effect deduced from the lower crust and upper mantle into consideration, we further calculated the postseismic $\triangle CFS$. The pattern of the postseismic $\triangle CFS$ is similar to

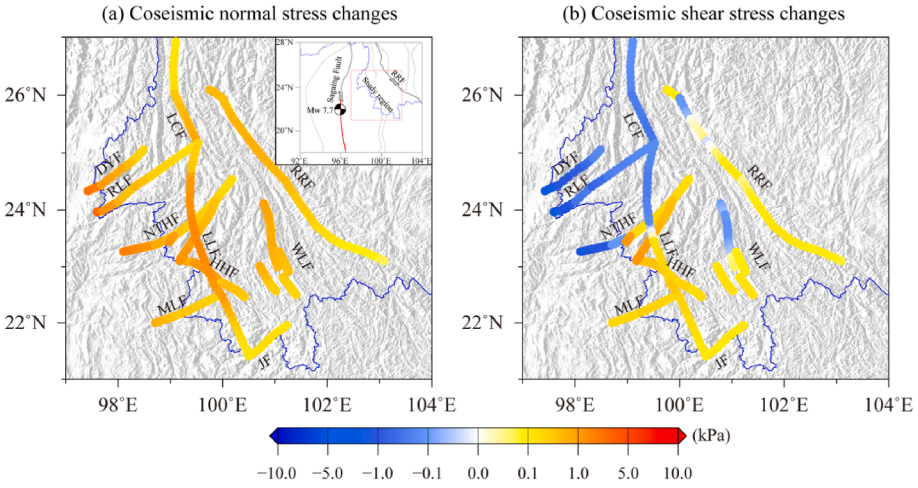

Fig. 4. Coseismic normal stress changes (a) and the coseismic shear stress changes (b) on the main active faults in the southwestern Yunnan region. The inset in the top right of the panel (a) marks the study region with respect to the M_W 7.7 mainshock and the Sagaing fault. The red line denotes the coseismic rupture length of ~500 km of the M_W 7.7 Myanmar earthquake.

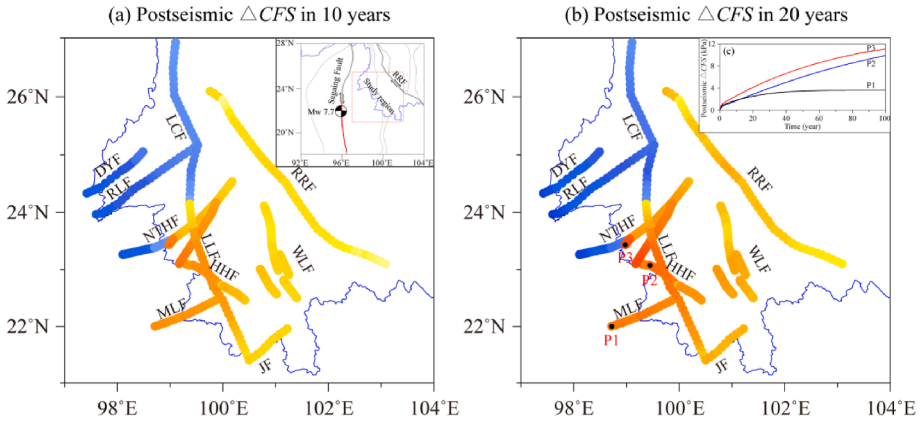

Fig. 5. Postseismic △*CFS* on main active faults in southwestern Yunnan region ($\mu' = 0.4$). Panels (a) and (b) represent the postseismic △*CFS* in 10 and 20 years derived from the postseismic viscoelastic relaxation effect following the Myanmar earthquake. The inset in the top right of the panel (a) marks the study region with respect to the M_W 7.7 mainshock and the Sagaing fault. The red line denotes the coseismic rupture length of ~500 km of the M_W 7.7 Myanmar earthquake. Panel (c) shows the post-seismic Δ*CFS* changing with time until 100 years at three points on the MLF, HHF, and NTHF near the Myanmar/China borders, respectively.

that of the coseismic △*CFS* (Fig. 5), suggesting that with the increasing elapsed time, the stress level continues to increase in the fault zone with the increased coseismic △*CFS*. The postseismic △*CFS* on the fault plane after 10 years' postseismic viscoelastic relaxation is equivalent to that of the coseismic △*CFS* (Fig. 5a). The postseismic △*CFS* derived from 20 years' postseismic viscoelastic relaxation reaches 5.5 kPa (Fig. 5b), suggesting that on the longer timescales of decades to centuries, the increasing stress change derived from postseismic viscoelastic relaxation effect can contribute more to the combined (co- and post-seismic) stress change (Fig. 5c).

4.2. *Auxiliary coseismic principal stress fields associated with the Myanmar M_W 7.7 earthquake*

The auxiliary stress fields (Fig. 6) show that, in most of the southwestern Yunnan region, the magnitude of the principal tensile stress is larger than the principal compressive stress. The orientation of the principal tensile stress is predominantly NE-SW in the northern part of the southwestern Yunnan region and shows a clockwise rotation to NW-SE in the south. The fault behavior is closely related to the stress regime, for these strike-slip dominated faults, the Nantinghe Fault and the Menglian Fault experience the additional coseismic sinistral strike-slip motion; The Longling-Lancang Fault, the Heihe Fault, the Red River Fault, and the Wuliangshan Fault experience the additional coseismic dextral strike-slip motion, which are all consistent with the tectonic active motion (Fig. 1b). On the contrary, the Dayingjiang Fault, the Ruili-Longling Fault, and the Lancangjiang Fault experience the opposite slip motion to tectonic active motion. All these coseismic additional slip motions are consistent with that reflected by the coseismic shear stress change (Fig. 4b).

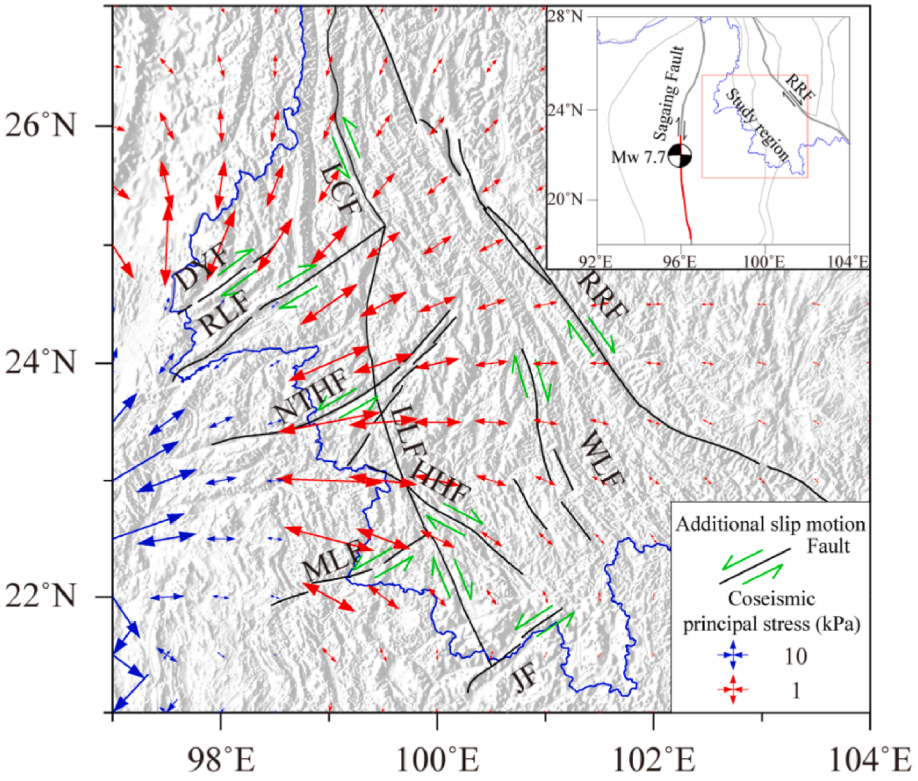

Fig. 6. Coseismic principal stress fields associated with the M_W 7.7 Myanmar earthquake. The pairs of green arrows represent the coseismic additional horizontal slip imparted by the auxiliary stress regime. The inset in the top right marks the study region with respect to the M_W 7.7 mainshock and the Sagaing fault. The red line denotes the coseismic rupture length of ~500 km of the M_W 7.7 Myanmar earthquake.

5. Discussion

In this study, we calculated the co- and post-seismic △*CFS* imparted by the M_W 7.7 Myanmar earthquake on major faults near the border between Myanmar and China. Our main findings were that several major faults, including the Longling-Lancang Fault, the Nantinghe Fault, the Menglian Fault, the Heihe Fault, and the Red River Fault experienced positive △*CFS*, while others, including the Dayingjiang Fault, the Ruili-Longling Fault, and the Lancangjiang Fault, experienced negative △*CFS* from the Myanmar mainshock. Before exploring the implications for seismic hazards in the adjacent southwestern Yunnan region in China, we first discussed the robustness of Coulomb stress changes and their sensitivities to different choices of parameters.

As shown in Eq. (1), the effective friction coefficient affects the contributions of the normal stress change to △*CFS*. To analyze the effect of different μ', we further calculate the coseismic △*CFS* with alternative values of $\mu' = 0.2$, 0.4, 0.6, and 0.8, respectively. The results demonstrate that the different μ' changes the magnitude of the △*CFS*, rather than the stress pattern (Fig. 7). Back to the coseismic normal stress change and shear stress change on main active faults (Fig. 4), we found that most of the faults plane experienced a significant coseismic tensile stress and positive shear stress change. In this scenario, the sign of △*CFS* is independent of the μ'. While for the Dayingjiang Fault, the Ruili-Longling Fault, and the Lancangjiang Fault which with significant negative coseismic Coulomb stress change, the absolute value of the coseismic shear stress change is larger than the coseismic normal stress change, and the shear stress change is the main factor in the △*CFS*, which is comparable to the Coulomb stress change imparted to fault imaged by focal mechanism. Thus, we suggested that the △*CFS* is generally robust for most faults with alternative values μ' ranging from 0 to 1. However, the △*CFS* sign changed from negative to positive signs for some fault segments (e.g., NTHF) near 24°N, indicating the sensitivities of the △*CFS* on different choices of μ'.

The seismic active southwestern Yunnan region has experienced strong historical earthquakes but has been quiet following the *M* 7.1 Menglian earthquake in 1995 (Li et al., 2020a), which aroused great concern about the seismic hazards on major active faults in this region. In these complex fault systems, Coulomb stress changes from other recent earthquakes provide one way to examine the earthquake potentials in the near future (Liu et al., 2011; Shi et al., 2020). In our previous study (Li et al., 2020a), we analyzed the total stress change (co-, post-, and inter-seismic) on the main active fault by integrating the $M \geq 6.7$ earthquakes in Sagaing Fault since 1929 and the $M \geq 6.7$ earthquakes in southwestern Yunnan region, and identified a significant total stress build-up on five segments distributed among the Nantinghe Fault, the Longling-Lancang Fault, the Heihe Fault, and the Menglian Fault. The occurrence of the M_W 7.7 Myanmar earthquake further cast positive Coulomb stress changes to these faults (Fig. 3), bringing them closer to their failure stage. According to Li et al. (2020a), the background tectonic loading rate of these faults is 1~2 kPa/yr. The coseismic effect of the M_W 7.7 Myanmar earthquake is equivalent to 1.5–3 years of tectonic loading. The post-seismic viscoelastic response will contribute to add more stress over the next few years (Fig. 5c), followed by gradual decay (Lei et al., 2013).

Geodetic inversion-derived slip deficit rates show that the northeastern trending faults have cumulated seismic moments capable of producing an earthquake of ~6.5, based on the latest earthquake and its elapsed time (Li et al., 2025). Moreover, based on the *b*-value in the Gutenberg-Ritcher magnitude-frequency relationship and distribution of historically strong earthquakes, Shao et al. (2015) suggested that the

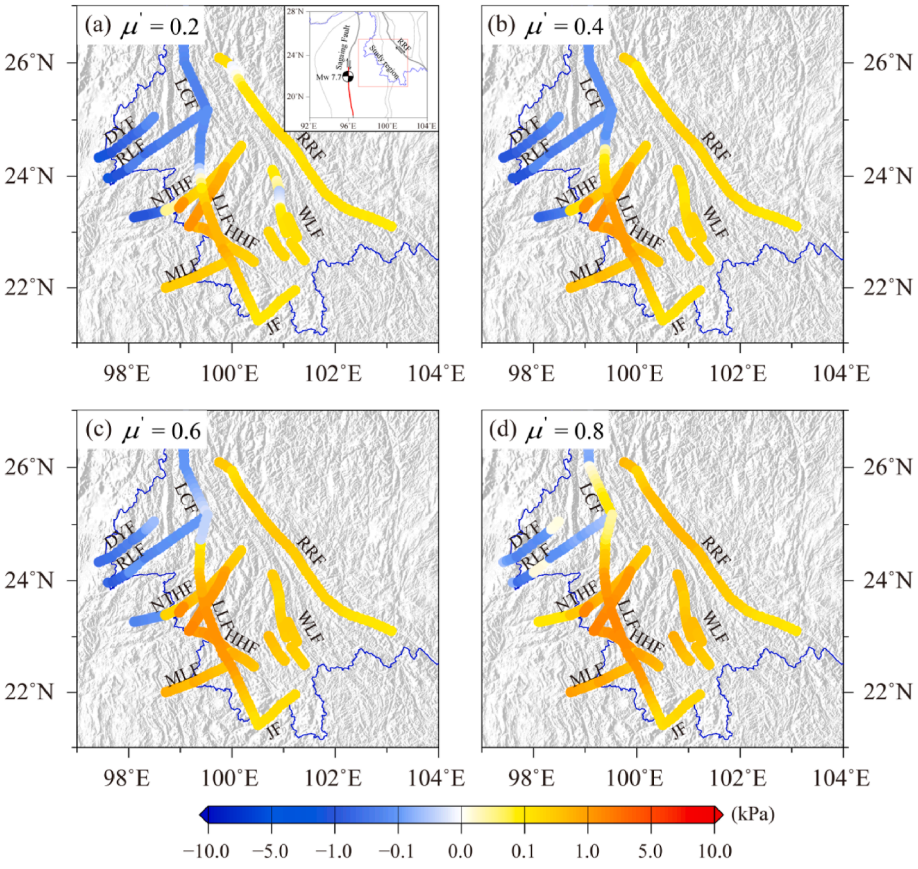

Fig. 7. Coseismic △*CFS* on main active faults in the southwestern Yunnan region with different apparent friction coefficients $\mu' = 0.2$ (a), 0.4 (b), 0.6 (c), and 0.8 (d), respectively. The inset in the top right marks the study region with respect to the M_W 7.7 mainshock and the Sagaing fault. The red line denotes the coseismic rupture length of ~500 km of the M_W 7.7 Myanmar earthquake.

Longling-Lancang Fault and the middle-east segment of the Menglian Fault have a potential for moderate-strong earthquake occurrence. Following our comprehensive analysis, we proposed that more attentions should be paid to the Longling-Lancang Fault, the Nantinghe Fault, the Menglian Fault, and the Heihe Fault, the candidates for future strong earthquakes in this region.

Magnetotelluric imaging shows a high-resistive structure extending through the entire upper crust in the southwestern Yunnan region (Chen et al., 2019). The Yingjiang moderate earthquake swarms in 2011 and the 1976 Longling doublets are all located in the transition zone of high resistivity (Ye et al., 2020), with a zone of low resistivity embedded in the depth range of 10 – 25 km. This mechanical decoupling benefits the strain energy accumulation and generation of large earthquakes (Liu et al., 2024, 2025; Zhang et al., 2022). With the plentiful three-dimensional deep electrical structure in the southwestern Yunnan region, we can analyze more earthquakes like the Gengma doublets in 1988, which can deepen our understanding of crustal stress heterogeneity and future seismic hazards in this region.

Coulomb stress change certainly influences the location and timing of the following earthquakes and can serve as a fundamental tool in seismic hazard analysis (Stein, 1999), owing to the positive correspondence with earthquake occurrence (Reasenberg and Simpson, 1992). However, other mechanisms of stress transfer, such as dynamic stress changes or time-dependent stress transfers, can also play an important role in earthquake triggering (Freed, 2005; Peng and Lei, 2025). We noted that due to limitations in basic data and models, there are still some different views on the seismogenic potential of this area. With the more precise community models in this region, such as the community velocity (Liu et al., 2023), and fault models, more accurate coseismic rupture model of the M_W 7.7 Myanmar earthquake (Wei et al., 2025), as well as more advanced numerical simulation techniques, a more comprehensive seismic hazard analysis is needed in the future.

6. Conclusions

In this study, we calculated the co- and post-seismic Coulomb stress change ($\triangle CFS$) imparted by the M_W 7.7 Myanmar earthquake to active faults in the southwestern Yunnan region and analyzed the seismic hazard.

(1) The Longling-Lancang Fault, the Nantinghe Fault, the Menglian Fault, the Heihe Fault, and the Red River Fault experience a coseismic stress increase, in which the coseismic $\triangle CFS$ reaches 3 kPa. The significant postseismic effect further increases the stress level on these faults, advancing the future strong earthquakes.
(2) The orientation of the coseismic auxiliary principal tensile stress is predominantly NE-SW in the northern part of the southwestern Yunnan region, and it shows clockwise rotation to NW-SE in the south, which controls the additional slip motion consistent with that reflected by the coseismic shear stress change.
(3) Combined with other geophysical and geodetic data, we propose that more attentions should be paid to the Longling-Lancang Fault, the Nantinghe Fault, the Menglian Fault, and the Heihe Fault.

CRediT authorship contribution statement

Yujiang Li: Writing – review & editing, Writing – original draft, Software, Funding acquisition, Conceptualization. **Cheng Yang:** Data curation. **Xingping Hu:** Writing – original draft, Formal analysis. **Jie Yuan:** Visualization, Investigation. **Rui Yao:** Investigation, Data curation. **Hong Li:** Writing – review & editing, Writing – original draft, Supervision.

Declaration of competing interest

The authors declare that they have no known competing financial interests or personal relationships that could have appeared to influence the work reported in this paper.

Author agreement and Acknowledgment

We appreciate the Chief Editor Zhigang Peng and three anonymous reviewers for their constructive comments and suggestions to improve our manuscript. This work was supported by the Deep Earth Probe and Mineral Resources Exploration-National Science and Technology Major Project (2024ZD1000703), National Natural Science Foundation of China (Grant Nos. 42274138, U23A2029, 41874116). Figures were plotted using the Generic Mapping Tools (Wessel et al., 2013).

Appendix A. Supplementary data

Supplementary data to this article can be found online at https://doi.org/10.1016/j.eqrea.2025.100397.

References

Bradley, K., Hubbard, J.A., 2025. Surface ruptures of the Myanmar M 7.7 earthquake mapped from space. Earthq. Insights. https://doi.org/10.62481/51b7df8c.
Chen, X., Ye, T., Cai, J., Wang, L., 2019. Refined techniques for data processing and two-dimensional inversion in magnetotelluric (VII): electrical structure and seismogenic environment of Yingjiang-Longling seismic area. Chin. J. Geophys. 62, 1377–1393.
Curray, J.R., 2005. Tectonics and history of the Andaman sea region. J. Asian Earth Sci. 25, 187–232. https://doi.org/10.1016/j.jseaes.2004.09.001.
Freed, A.M., 2005. Earthquake triggering by static, dynamic, and postseismic stress transfer. Annu. Rev. Earth Planet Sci. 33, 335–367. https://doi.org/10.1146/annurev.earth.33.092203.122505.
Fu, B., Walker, R., Sandiford, M., 2011. The 2008 Wenchuan earthquake and active tectonics of Asia. J. Asian Earth Sci. 4, 797–804. https://doi.org/10.1016/j.jseaes.2011.01.003.
Hall, S., 2023. What Turkey's earthquake tells us about the science of seismic forecasting. Nature 615, 388–389. https://doi.org/10.1038/d41586-023-00685-y.
Harris, R.A., 1998. Introduction to special section: stress triggers, stress shadows, and implications for seismic hazard. J. Geophys. Res. 103, 24347–24358. https://doi.org/10.1029/98JB01576.
Hu, X.P., Zang, A., Heidbach, O., Cui, X.F., Xie, F.R., Chen, J.W., 2017. Crustal stress pattern in China and its adjacent areas. J. Asian Earth Sci. 149, 20–28. https://doi.org/10.1016/j.jseaes.2017.07.005.
Hubert-Ferrari, A., Barka, A., Jacques, E., Nalbant, S.S., Meyer, B., Armijo, R., Tapponnier, P., King, G.C., 2000. Seismic hazard in the Marmara sea region following the 17 August 1999 Izmit earthquake. Nature 404, 269–273. https://doi.org/10.1038/35005054.
Hurukawa, N., Maung Maung, P., 2011. Two seismic gaps on the Sagaing Fault, Myanmar, derived from relocation of historical earthquakes since 1918. Geophys. Res. Lett. 38. https://doi.org/10.1029/2010GL046099.
Inoue, N., Yamaguchi, R., Yagi, Y., Okuwaki, R., Enescu, B.D., Tadapansawut, T., 2025. A multiple asymmetric bilateral rupture sequence derived from the peculiar teleseismic P-waves of the 2025 Myanmar earthquake. Seismica, in review. https://doi.org/10.26443/seismica.v4i1.1691.
King, G.C., Stein, R.S., Lin, J., 1994. Static stress changes and the triggering of earthquakes. Bull. Seismol. Soc. Am. 84, 935–953. https://doi.org/10.1785/BSSA0840030935.
Kundu, B., Gahalaut, V., 2012. Earthquake occurrence processes in the Indo-Burmese wedge and Sagaing fault region. Tectonophysics 524, 135–146. https://doi.org/10.1016/j.tecto.2011.12.031.
Le Dain, A.Y., Tapponnier, P., Molnar, P., 1984. Active faulting and tectonics of Burma and surrounding regions. J. Geophys. Res. 89, 453–472. https://doi.org/10.1029/JB089iB01p00453.
Lei, X.L., Ma, S.L., Su, J.R., Wang, X.L., 2013. Inelastic triggering of the 2013 M_W 6.6 Lushan earthquake by the 2008 M_W 7.9 Wenchuan earthquake. Seismol. Geol. 35, 411–422. https://doi.org/10.3969/j.issn.0253-4967.2013.02.019.
Li, Y., Liu, H., Yang, C., 2023. Revisiting the seismic hazards of faults surrounding the 2022 M_S 6.8 Luding earthquake, Sichuan, China. Geomat. Nat. Hazards Risk 14, 2272569. https://doi.org/10.1080/19475705.2023.2272569.
Li, Y., Shan, X., Qu, C., Zhang, G., Wang, X., Xiong, H., 2025. Slip deficit rate and seismic potential on crustal faults in Tibet. Geophys. Res. Lett. 52, e2024GL112122. https://doi.org/10.1029/2024GL112122.
Li, Y.J., Huang, L.Y., Ding, R., Yang, S.X., Liu, L., Zhang, S.M., Liu, H.Q., 2021. Coulomb stress changes associated with the M 7.3 Maduo earthquake and implications for seismic hazards. Nat. Hazards 1, 95–101. https://doi.org/10.1016/j.nhres.2021.06.003.

Li, Y.J., Shao, Z.G., Shi, F.Q., Chen, L.W., 2020a. Stress evolution on active faults in the southwestern Yunnan region, southeastern Tibetan Plateau, and implications for seismic hazard. J. Asian Earth Sci. 200, 104470. https://doi.org/10.1016/j.jseaes.2020.104470.

Li, Y.J., Shi, F.Q., Zhang, H., Wei, W.X., Xu, J., Shao, Z.G., 2020b. Coulomb stress change on active faults in Sichuan-Yunnan region and its implications for seismic hazard. Seismol. Geol. 42, 526–546.

Lindsey, E.O., Wang, Y., Aung, L.T., Chong, J.-H., Qiu, Q., Mallick, R., Feng, L., Aung, P. S., Tin, T.Z.H., Min, S.M., 2023. Active subduction and strain partitioning in western Myanmar revealed by a dense survey GNSS network. Earth Planet Sci. Lett. 622, 118384. https://doi.org/10.1016/j.epsl.2023.118384.

Liu, H., Gan, W., Li, Y., Li, Z., Liu, L., Zhang, L., Liang, S., Zhang, K., Li, Y., Dai, C., 2025. Mechanism of crustal deformation around the Lajishan-Jishishan tectonic belt, NE tibet, and implications for occurrence of the 2023 Jishishan M_S 6.2 earthquake. J. Asian Earth Sci. 279, 106449. https://doi.org/10.1016/j.jseaes.2024.106449.

Liu, H., Li, Y., Yang, C., Chen, L., 2024. Stress heterogeneity in the eastern Tibetan Plateau and implications for the present-day plateau expansion. Tectonophysics 890, 230513. https://doi.org/10.1016/j.tecto.2024.230513.

Liu, M., Stein, S., Wang, H., 2011. 2000 years of migrating earthquakes in North China: how earthquakes in midcontinents differ from those at plate boundaries. Lithosphere 3, 128–132. https://doi.org/10.1130/L129.1.

Liu, Y., Yu, Z., Zhang, Z., Yao, H., Wang, W., Zhang, H., Fang, H., Fang, L., 2023. The high-resolution community velocity model V2.0 of southwest China, constructed by joint body and surface wave tomography of data recorded at temporary dense arrays. Sci. China Earth Sci. 66, 2368–2385.

Maurin, T., Masson, F., Rangin, C., Min, U.T., Collard, P., 2010. First global positioning system results in northern Myanmar: constant and localized slip rate along the Sagaing fault. Geology 38, 591–594. https://doi.org/10.1130/G30872.1.

Nalbant, S.S., Hubert, A., King, G.C., 1998. Stress coupling between earthquakes in northwest Turkey and the north Aegean Sea. J. Geophys. Res. 103, 24469–24486. https://doi.org/10.1029/91JB01021.

Nalbant, S.S., McCloskey, J., Steacy, S., Barka, A.A., 2002. Stress accumulation and increased seismic risk in eastern Turkey. Earth Planet Sci. Lett. 195, 291–298. https://doi.org/10.1029/98JB01491.

Nielsen, C., Chamot-Rooke, N., Rangin, C., 2004. From partial to full strain partitioning along the Indo-Burmese hyper-oblique subduction. Mar. Geol. 209, 303–327. https://doi.org/10.1016/j.margeo.2004.05.001.

Panda, D., Kundu, B., Gahalaut, V.K., Rangin, C., 2018. Crustal deformation, spatial distribution of earthquakes and along strike segmentation of the Sagaing Fault, Myanmar. J. Asian Earth Sci. 166, 89–94. https://doi.org/10.1016/j.jseaes.2018.07.029.

Parsons, T., Ji, C., Kirby, E., 2008. Stress changes from the 2008 Wenchuan earthquake and increased hazard in the Sichuan basin. Nature 454, 509–510. https://doi.org/10.1038/nature07177.

Peng, Z., Lei, X., 2025. Physical mechanisms of earthquake nucleation and foreshocks: cascade triggering, aseismic slip, or fluid flows? Earthq. Res. Adv. 5, 100349. https://doi.org/10.1016/j.eqrea.2024.100349.

Peng, Z., Mach, P., Lei, X., Wang, D., Si, X., Zhong, Q., Ding, C., Deng, Y., Qin, M., Miao, S., 2025. Preliminary results on the main rupture properties, aftershock activities and remotely triggered seismicity associated with the 2025 M 7.7 Sagaing Fault earthquake in Myanmar. Earthq. Res. Adv., in review. https://doi.org/10.31223/X5BQ7D.

Rangin, C., Maurin, T., Masson, F., 2013. Combined effects of Eurasia/Sunda oblique convergence and East-Tibetan crustal flow on the active tectonics of Burma. J. Asian Earth Sci. 76, 185–194. https://doi.org/10.1016/j.jseaes.2013.05.018.

Reasenberg, P.A., Simpson, R.W., 1992. Response of regional seismicity to the static stress change produced by the Loma Prieta earthquake. Science 255, 1687. https://doi.org/10.1126/science.255.5052.1687.

Shan, B., Xiong, X., Wang, R., Zheng, Y., Yang, S., 2013. Coulomb stress evolution along Xianshuihe–Xiaojiang fault system since 1713 and its interaction with Wenchuan earthquake, May 12, 2008. Earth Planet Sci. Lett. 377–378, 199–210. https://doi.org/10.1016/j.epsl.2013.06.044.

Shao, Y.X., Yuan, D.Y., Liang, M.J., 2015. Seismic risk assessment of Longling-Lancang fault zone, southwestern Yunnan. Acta Seismol. Sin. 37, 1011–1023.

Shao, Z.G., Xu, J., Ma, H.S., Zhang, L.P., 2016. Coulomb stress evolution over the past 200 years and seismic hazard along the Xianshuihe fault zone of Sichuan, China. Tectonophysics 670, 48–65. https://doi.org/10.1016/j.tecto.2015.12.018.

Shi, F.Q., Zhang, H., Shao, Z.G., Xu, J., Shao, H.C., Li, Y.J., 2020. Coulomb stress evolution and stress interaction among strong earthquakes in North China. Chin. J. Geophys. 63, 3338–3354.

Shi, X., Wang, Y., Sieh, K., Weldon, R., Feng, L., Chan, C.H., Liu-Zeng, J., 2018. Fault slip and GPS velocities across the Shan Plateau define a curved southwestward crustal motion around the eastern Himalayan syntaxis. J. Geophys. Res. 123, 2502–2518. https://doi.org/10.1002/2017JB015206.

Socquet, A., Simons, W., Vigny, C., McCaffrey, R., Subarya, C., Sarsito, D., Ambrosius, B., Spakman, W., 2006. Microblock rotations and fault coupling in SE Asia triple junction (Sulawesi, Indonesia) from GPS and earthquake slip vector data. J. Geophys. Res. 111. https://doi.org/10.1029/2005JB003963.

Stein, R.S., 1999. The role of stress transfer in earthquake occurrence. Nature 402, 605–609. https://doi.org/10.1038/45144.

Stein, R.S., Barka, A.A., Dieterich, J.H., 1997. Progressive failure on the North Anatolian fault since 1939 by earthquake stress triggering. Geophys. J. Int. 128, 594–604. https://doi.org/10.1111/j.1365-246X.1997.tb05321.x.

Taylor, M., Yin, A., 2009. Active structures of the Himalayan-Tibetan orogen and their relationships to earthquake distribution, contemporary strain field, and Cenozoic volcanism. Geosphere 5, 199–214. https://doi.org/10.1130/GES00217.1.

Tin, T.Z.H., Nishimura, T., Hashimoto, M., Lindsey, E.O., Aung, L.T., Min, S.M., Thant, M., 2022. Present-day crustal deformation and slip rate along the southern Sagaing fault in Myanmar by GNSS observation. J. Asian Earth Sci. 228, 105125. https://doi.org/10.1016/j.jseaes.2022.105125.

Toda, S., Stein, R.R., 2025. One-month earthquake forecast for western Myanmar following the devastating magnitude 7.7 Mandalay shock. Temblor. http://doi.org/10.32858/temblor.360.

Tun, S.T., Watkinson, I.M., 2017. Chapter 19: the Sagaing Fault, Myanmar. In: Barber, A. J., Zaw, K., Crow, M.J. (Eds.), Myanmar: Geology, Resources and Tectonics. Geological Society, London, Memoirs. https://doi.org/10.1144/m48.19.

Vigny, C., Socquet, A., Rangin, C., Chamot-Rooke, N., Pubellier, M., Bouin, M.N., Bertrand, G., Becker, M., 2003. Present-day crustal deformation around Sagaing fault, Myanmar. J. Geophys. Res. 108, 2533. https://doi.org/10.1029/2002JB001999.

Wan, Y.G., Wu, Z.L., Zhou, G.W., Huang, J., 2000. Stress triggering between different rupture events in several earthquakes. Acta Seismol. Sin. 13, 607–615.

Wang, K.L., Hu, Y., He, J.H., 2012. Deformation cycles of subduction earthquakes in a viscoelastic Earth. Nature 484, 327–332. https://doi.org/10.1038/nature11032.

Wang, R., Lorenzo-Martín, F., Roth, F., 2006. PSGRN/PSCMP—a new code for calculating co-and post-seismic deformation, geoid and gravity changes based on the viscoelastic-gravitational dislocation theory. Comput. Geosci. 32, 527–541. https://doi.org/10.1016/j.cageo.2005.08.006.

Wang, Y., Sieh, K., Tun, S.T., Lai, K.Y., Myint, T., 2014. Active tectonics and earthquake potential of the Myanmar region. J. Geophys. Res. 119, 3767–3822. https://doi.org/10.1002/2013JB010762.

Wei, S., Wang, X., Li, C., Zeng, H., Ma, Z., Shi, Q., Chen, L., 2025. Supershear rupture sustained through a thick fault zone in the 2025 Mw 7.8 Mandalay earthquake. Science 390 (6772), 468–475.

Wessel, P., Smith, W.H., Scharroo, R., Luis, J., Wobbe, F., 2013. Generic mapping tools: improved version released. Eos Trans. Am. Geophys. Union 94, 409–410. https://doi.org/10.1002/2013EO450001.

Wu, X.P., Hu, X.L., Bouchon, M., Huang, Y., Hu, J.F., Xie, C.D., Wang, S.J., Hu, Y., 2007. Complete Coulomb stress changes induced by the M_S 7.6 earthquake in Lancang-Gengma, Yunnan and triggering of aftershocks by dynamic and static stress. Sci. China Earth Sci. 50, 1655–1662.

Xiong, X., Shan, B., Zhou, Y.M., Wei, S.J., Li, Y.D., Wang, R.J., Zheng, Y., 2017. Coulomb stress transfer and accumulation on the Sagaing Fault, Myanmar over the past 110 years and its implications for seismic hazard. Geophys. Res. Lett. 44, 4781–4789. https://doi.org/10.1002/2017GL072770.

Ye, T., Chen, X., Huang, Q., Zhao, L., Zhang, Y., Uyeshima, M., 2020. Bifurcated crustal channel flow and seismogenic structures of intraplate earthquakes in western Yunnan, China as revealed by three-dimensional magnetotelluric imaging. J. Geophys. Res. 125, e2019JB018991. https://doi.org/10.1029/2019JB018991.

Zhang, G.W., Li, Y.J., Hu, X.P., 2022. Nucleation mechanism of the 2021 M_W 7.4 Maduo earthquake, NE Tibetan Plateau: insights from seismic tomography and numerical modeling. Tectonophysics 839, 229528. https://doi.org/10.1016/j.tecto.2022.229528.

Zhang, P., Deng, Q., Zhang, G., Ma, J., Gan, W., Min, W., Mao, F., Wang, Q., 2003. Active tectonic blocks and strong earthquakes in the continent of China. Sci. China, Ser. D Earth Sci. 46, 13–24. https://doi.org/10.1360/03dz0002.